Surface & Coatings Technology 286 (2016) 365–375

Contents lists available at ScienceDirect

Surface & Coatings Technology

journal homepage: www.elsevier.com/locate/surfcoat

Enhancement of high temperature oxidation resistance and spallation resistance of SiC-self-healing thermal barrier coatings

Taoyuan Ouyang [1], Xuanwei Fang [1], Ying Zhang [1], Dawei Liu [1], Yan Wang [1], Shuaijie Feng [1], Tong Zhou [1], Shuizhou Cai *, Jingpin Suo **

State Key Laboratory of Mould Technology, Institute of Materials Science and Engineering, Huazhong University of Science and Technology, 1037 Luoyu Road, Wuhan, PR China

ARTICLE INFO

Article history:
Received 20 October 2015
Revised 14 December 2015
Accepted in revised form 16 December 2015
Available online 19 December 2015

Keywords:
TBC
Self-healing
SiC
Oxidation resistance
Spallation resistance

ABSTRACT

Thermal barrier coatings (TBCs) are extensively used to protect metallic blades in gas-turbine engines where the operating conditions include an aggressive environment at high temperatures. The most important factor controlling TBC durability is the growth of a thermally grown oxide (TGO) layer which is formed during high temperature oxidation. To improve the oxidation resistance of conventional TBC, the SiC-self-healing coating, named the SAZ coating, was prepared by air plasma spray (APS) technique on the top of the classic bilayer TBC (YSZ TBC), which consist of the bond coating (BC) and the YSZ coating. Cracks allow SiC particles locating on the crack outside surface to react with the oxygen in the atmosphere at the temperature above 720 °C resulting in healing. As oxidation progress, the crack surfaces are covered with the formed oxide. Finally, the space between the crack surfaces is completely or incompletely filled with the formed oxide. The sealing effect enhanced the oxygen diffusion resistance of SAZ coatings, therefore the partial pressure of oxygen at the BC-YSZ interface of SAZ TBC samples would be lower than of YSZ TBC samples. The oxidation and spallation resistance of the SAZ TBC samples will be enhanced because the growth rate of TGO is slower due to the low partial pressure of oxygen. The high temperature cyclic oxidation tests performed at 1127 °C was carried out to investigate the oxidation and spallation resistance of the SAZ TBC. The results demonstrated that the mass gain of SAZ TBC samples, which was related to oxidation resistance, was 63.29% of YSZ TBC samples, and the mass loss of SAZ TBC samples, which was related to spallation resistance, was 56.08% of YSZ TBC samples.

1. Introduction

Thermal barrier coatings (TBC) are comprised of four layers: 1) the substrate, 2) the bond-coat (BC), 3) the thermally grown oxide (TGO), and 4) the ceramic top-coat (TC) [1]. The TGO layer is formed at the TC–BC interface at an elevated temperature. TGO acts as an oxidation barrier to suppress the formation of other detrimental oxides during any extended thermal exposure in service [2]; in other words, in the primary stages of service, the TGO helps protect the substrate from oxidation and improves the durability of TBCs. Out-of-plane stresses, however, which normally develop at BC–TC interface undulations, increase as the TGO thickens until they cause cracking within the brittle ceramic coatings and fracture at the interfaces. These mechanisms combined can then induce TBC failure [3].

Several different methods have been proposed in recent years to improve the oxidation resistance and lifetime of TBCs. Researchers have attempted to improve TBC lifetime by employing dense YSZ coating structures under very low pressure plasma spray (VLPPS), electrodepositing, and laser re-melting, for example [4–6]. The dense nanostructure of YSZ layers plays an effective role in reducing oxygen permeation [4], and creates a TBC with favorable thermal shock resistance due to reduced TGO growth in the YSZ/BC interface [5]. Several modified BCs have also been proposed, including those with Hf, Zr [7], Pt [8], and nanostructure oxide [9]added to the BCs to enhance the oxidation resistance of TBCs. In addition to modified YSZ coatings and BCs, many researchers have worked to develop other types of coatings that improve oxidation resistance after being integrated into the TBC system [10–16]. Many of these methods include the application of Al_2O_3, which benefits oxidation resistance because the oxygen diffusion coefficient of Al_2O_3 is very small (~10^{-12} cm^2/s at 1400 °C.)

Self-healing materials include polymers [17–19], metals [20–23], ceramics [24–28], and their composites [29–32] that when damaged through thermal, mechanical, ballistic, or other means have the ability

* Corresponding author.
** Correspondence to: School of Materials Science and Engineering, Huazhong University of Science and Technology, 430070 Wuhan, Hubei, PR China.
E-mail addresses: ouyangty@foxmail.com (T. Ouyang), 247836706@qq.com (X. Fang), 123456@qq.com (Y. Zhang), davy1062@163.com (D. Liu), 249138384@qq.com (Y. Wang), 1425480235@qq.com (S. Feng), 543665596@qq.com (T. Zhou), shuizhoucai@163.com (S. Cai), jinpingsuo@hust.edu.cn (J. Suo).
[1] School of Material Science and Technology, Huazhong University of Science & Technology, 1037 Luoyu Road, Wuhan, PR China.

http://dx.doi.org/10.1016/j.surfcoat.2015.12.054
0257-8972/

to restore their own original properties [33]. Self-healing materials are often used to produce anticorrosion coatings [34–37] and polymer coatings [38–41]. There are only a few patents (such as CN103553597-A, US2015159492-A1, US7662684-N) for self-healing TBCs, specifically.

Self-healing material may represent an innovation solution to problems with porous coatings, because the porous structure of ceramic coatings prepared by APS is inevitable, and the pores in coatings provide fast-diffusion paths for oxygen transportation. If the pores and cracks are filled by a self-healing agent, the diffusion of oxygen should be much slower. For example, Raj et al. [42]studied lightweight self-healing ceramic composites for application in high-temperature aircraft engines, and found that SiC and its oxides had sufficient plasticity to reduce crack propagation and self-healing capabilities, filling surface-connected cracks to prevent oxygen ingress.

The present study developed a SiC-self-healing TBC in effort to improve the oxidation resistance and spallation resistance of the TBC system. We first elucidated the oxidation mechanism of the self-healing agent and its filling and sealing effect, then investigated the TBC's oxidation behavior at high temperatures. To conclude the study, crack evolution in TGOs and composite coatings were compared and analyzed.

2. Materials and methods

2.1. Coating preparation

Disk-shaped substrate specimens, with diameter of 20 mm and thickness of 5 mm, were cut from a GH4169 alloy bar. The nominal composition of GH4169 is provided in Table 1. Before the coatings were sprayed, all the substrates were blasted with compressed air for enhancing adhesion and removing rust on the surface of the substrates.

Two types of TBC samples, the YSZ TBC and the SAZ TBC, were fabricated using the air plasma spraying (APS) system. The schematic layer structure of the composite coatings is shown in Fig. 2. The cross-section SEM morphologies for as-sprayed samples are shown in Fig. 4 and their corresponding XRD traces from the surfaces are shown in Fig. 5.

NiCoCrAlY, the composition of which is given in Table 2 [43], was used to spray the BC. NiCoCrAlY powder grains had diameter of about 40–150 μm. The YSZ layer was made of 8 wt.% Y_2O_3–ZrO_2 (8YSZ), with powder grains 60–80 μm in diameter. SAZ powders had diameter of 40–60 μm, and were comprised of 6 wt.% SiC, 56 wt.% 8YSZ, and 38 wt.% Al_2O_3. The raw powders of SiC, 8YSZ, and Al_2O_3 were 60 nm in diameter; they were sprayed dry into the composite SAZ powder. The spraying parameters for ceramic coatings and metallic coatings are listed in Table 3.

2.2. Microstructural characterization

TBC microstructure was characterized by scanning electron microscopy (SEM). The specimens were impregnated in vacuum conditions using cold mounting and embedding resins (HY-607 AB), which protected the coatings during cross-section polishing. After the experiments, the TBC thickness of each sample was evaluated as the average of 20 values along the entire specimen according to SEM images. The percentage of TGO in the BCs was analyzed with Image-Pro Plus 6.0 (IPP) software, which distinguished the percentage of TGO in the BCs in different composites. SAZ layer porosity before and after heat treatment was measured by the same means.

Table 1
The nominal chemical composition of GH4169 (wt.%).

C	Cr	Ni	Co	Mo	Al	Ti	Fe
≤0.08	17.0–21.0	50–55.0	≤1.0	2.80–3.30	0.30–0.70	0.75–1.15	Rest

Table 2
The chemical composition of NiCoCrAlY (wt.%).

Ni	Al	Co	Cr	Y
46.55	13	23	17	0.45

2.3. Image Pro Plus

Image Pro Plus (IPP) software effectively provides advanced image processing features for analysis. Fig. 1a shows an original SEM image for YSZ coatings, and Fig. 1b shows the processed image. The software readily provided porosity information, then the map information allowed us to calculate area percentages.

2.4. Electrochemical test

A three-electrode electrochemical cell was used for electrochemical measurements, with a saturated Ag/AgCl electrode (+0.205 V vs. SHE) as the reference electrode, platinum wire as the counter electrode, and a coating sample as the working electrode. The exposed area of samples was 3.14 cm^2. EIS measurements were repeatedly performed in 3.5 wt.% NaCl solution after different exposure periods in the frequency range 10^5–10^{-2} Hz, under perturbation amplitude of 20 mV. [44].

A potential scanning rate of 1 mV/s was adopted to gather all potentiodynamic measurements. The potential range was from −800 mV to 0 mV. Corrosion current densities (I_{corr}) and corrosion potentials (E_{corr}) were evaluated according to the intersection of the linear anodic and cathodic branches of the polarization curves (i.e., the Tafel extrapolation, shown in Fig. 3) and were given by the ZView software.

2.5. Self-healing process

A self-healing heat treatment was applied to investigate self-healing effect of the samples. The SAZ TBC samples were self-healing heat-treated in air in a furnace at 720 °C for a period of 10 h. The mass gain of SAZ TBC samples was weighed using an electronic analytical balance (0.1 mg accuracy) every hour of the treatment. To investigate the filling and sealing effect of healed coatings, the electrochemical test was conducted to investigate the corrosion behavior of SAZ TBC samples before and after heat treatment.

2.6. High-temperature cyclic oxidation testing

Cyclic isothermal oxidation tests were also performed for three samples of the YSZ TBC, the SAZ TBC and three samples only coated with NiCoCrAlY in the same muffle furnace at 1127 °C and 1 atm for 20 h. Prior to the tests, alumina crucibles were pre-heated until reaching a constant weight. After every 1 h of exposure, specimens and crucibles were furnace-cooled to ambient temperature, then their mass gain and mass loss were recorded. Mass gain value, which is related to TBC oxidation behavior, was calculated by weighing the specimen with the crucible; mass loss value, which is related to TBC oxidation spallation, was recorded by weighing specimens without crucibles. Both the mass

Table 3
Deposition parameters for the thermal sprayed APS.

	Ceramic coatings	Metallic coatings
Voltage (V)	70–75	65–70
Current (A)	500	450
Spray dist (mm)	90	140
H2 (L/min)	3	–
N2 (L/min)	8	8
Ar (L/min)	25	25
Feed rate (g/min)	20 ± 2	30 ± 2
Cooling water (°C)	25	25

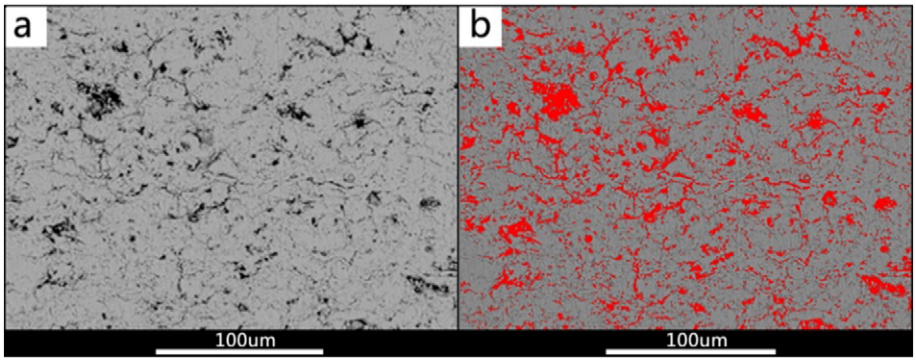

Fig. 1. Typical cross-section morphologies of YSZ coatings: (a) original SEM image and (b) processed image by IPP.

gain and mass loss were recorded using an analytical balance with 0.1 mg accuracy, and every data was the average value of three samples.

3. Results

3.1. Microstructure and phase composition for feedstock

Fig. 4 shows the cross-section morphologies of as-sprayed YSZ TBC and SAZ TBC samples. According to these images, both YSZ TBCs and SAZ TBCs were comprised of a ~50 μm-thick NiCoCrAlY bond coating and a ~150 μm-thick 8YSZ coating. The SAZ coatings were ~20 μm in thickness.

XRD traces from the surfaces of as-sprayed samples are shown in Fig. 5. For the conventional TBC specimens, XRD traces at the surface exhibited peaks associated with cubic ZrO_2 (Fm3m space group, a = 0.513 nm), as the majority phase, together with peaks from tetragonal ZrO_2 (P42/nmc space group, a = 0.364 nm and c = 0.527 nm). The top SiC-self-healing coating showed peaks from Al_2O_3, ZrO_2 and SiC. The peaks for Si and C were detected on the surface of SAZ TBC samples (Fig. 6a) by EDS (Fig. 6b). Due to the massive presence of Al and Si oxides on the surface, the element of C is beneath the thick oxide layer, so the peak for C is weak.

3.2. Self-healing process

Specimens before and after self-healing heat treatment and isothermal oxidation in the furnace at 720 °C for a period of 10 h are shown in Fig. 7. The SAZ–YSZ interface before and after heat treatment is shown in Fig. 8, and mass changes of YSZ TBC and SAZ TBC samples during the self-healing process are shown in Fig. 9. Electrochemical test results are shown in Fig. 10.

Compared to the corrosion current densities for other samples, self-healed SAZ TBCs showed higher resistance. Their corresponding corrosion current densities are 2.06×10^{-7} A/cm^2 for the as-sprayed SAZ TBC sample and 6.04×10^{-8} A/cm^2 for the healed SAZ TBC sample. The filling and sealing effect reduced 70.68% corrosion current density.

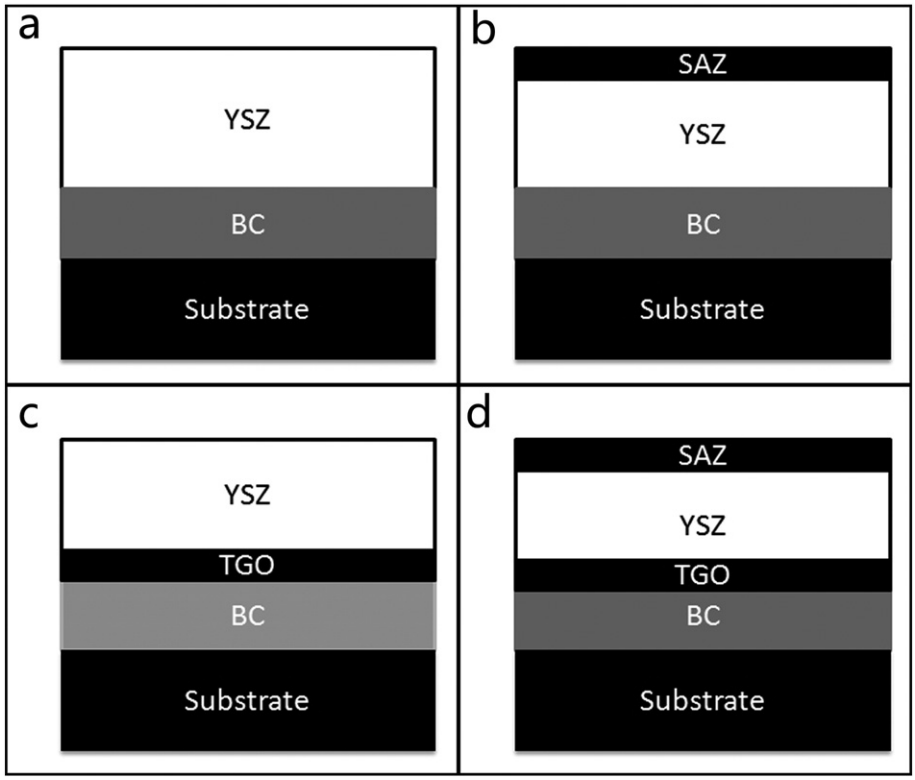

Fig. 2. Schematic draw of (a) the YSZ TBC structure, (b) the SAZ TBC structure, (c) the YSZ TBC structure with TGO and (d) the SAZ TBC structure with TGO.

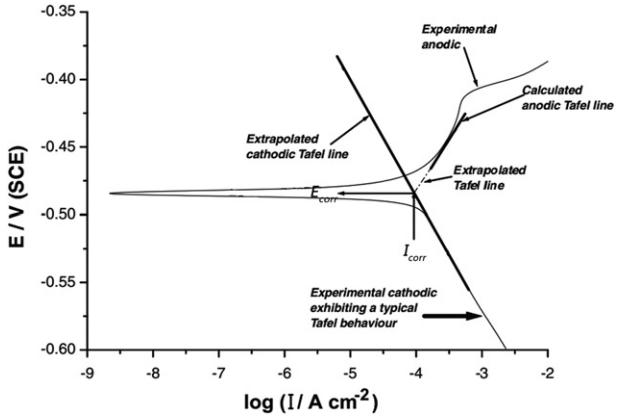

Fig. 3. Schematic draw of polarization curve and Tafel extrapolation.

3.3. High-temperature cyclic oxidation test

Oxygen penetrated through the top coatings during exposure at high temperatures in air, where a TGO layer was formed at the interface between bond coatings and YSZ coatings [3]. The isothermal oxidation weight gain and weight loss kinetic curves of the composite TBCs at 1127 °C in the furnace for the total period of 20 h are shown in Fig. 11a and b, respectively.

Fig. 12 shows a SEM image of the cross-section morphologies for conventional TBC and SAZ after 5, 10, 15, and 20 isothermal oxidation cycles. The oxidation resistance of SAZ TBC samples was clearly better than those of YSZ TBC, because the oxide grew faster in YSZ TBC samples. The TGO thickness of samples in the initial 10 h of oxidation, and the TGO area percentage of samples in different stages, were calculated by IPP analysis as listed in Table 4. Coating spallation first occurred when YSZ TBC had gone through 14 cycles, 8 cycles, and 11 cycles for the three samples, respectively. SAZ TBC spallation during high-temperature oxidation cyclic testing first occurred when the first two samples had gone through 18 cycles and 18 cycles, respectively, but the third sample did not show any spallation even after 20 cycles. The high-temperature cyclic oxidation test did not stop until 20th high temperature oxidation cycle for most specimens, even if the SAZ TBC samples or the YSZ TBC samples had peeled off.

Fig. 14 shows where the TGO involved two types of oxide. The substrate is marked by "b" in Fig. 14(a); the EDS results (Fig. 14b) supported this observation. The chromic oxide TGO was in amorphous (marked as "c" in Fig. 14a) and the aluminum TGO was in the shape of a strip ("d" in Fig. 14a). Element analyses of the samples are shown in Fig. 14c and d, as well.

Cracks propagating through YSZ and TGO were found both in YSZ TBC and SAZ TBC samples (Fig. 15). IPP software analysis provided the TGO thickness and total TGO percentage of failed samples, as listed in Table 4.

4. Discussion

4.1. Self-healing process mechanism

Theoretically, SiC self-healing agent in the coatings reacts with oxygen and oxidations its corresponding oxide, SiO_2, at temperatures above 700 °C. For this reason, we conducted a low-temperature oxidation test at 720 °C in effort to better understand the self-healing mechanism at work in our samples. The filling and sealing effects were the result of oxidation reactions — when oxygen was transported through the self-healing coatings, the self-healing agent healed cracks in the sample by oxidation. The volume expansion can be calculated by the following formula:

$$V_{\text{self-healing}} = M_{SiO_2} \times \rho_{SiC} / (M_{SiC} \times \rho_{SiO_2}) - 1 \quad (1)$$

where V, M, and ρ denote volume, molar quantity, and density, respectively. The densities of SiC and SiO_2 were 3.2 g cm^{-3} and 2.2 g cm^{-3}, respectively, so the SiC material expanded by 118% (in theory.)

The oxidation kinetic curves of SAZ TBC and YSZ TBC samples processed at 720 °C for 10 h are shown in Fig. 9. The mass of SAZ TBC samples continued to grow by 0.25 mg/cm^2 in total in the first 3 h, but there was relatively little mass change in the last 7 h. The YSZ TBC samples showed almost no change in mass throughout the entire experiment. The YSZ coatings, BCs, and substrates not responsible for mass gain during the 720 °C oxidation test, but the SAZ coatings were. The oxidation of self-healing agent was the cause of mass gain, and oxidation had finished after 10 h of heat treatment. The filling and sealing effect caused by this oxidation of self-healing agent had a few important implications.

Cross-section morphologies (Fig. 7) before and after heat treatment revealed filling and sealing effects at the microstructure level. The cross-section morphologies and surface morphologies of SAZ coatings before and after 10-hour heat treatment (Fig. 7) were analyzed by IPP software, which showed that porosity in SAZ coatings decreased 76.71%, from 9.19% to 2.14% (Table 4), after oxidation. In effect, heat treatment provoked filling and sealing in the self-healing coatings, evidenced by the filled and sealed pores and micro-cracks shown in the sample morphologies. In addition, the volume expansion that resulted from self-healing at temperatures above 720 °C, did not damage coating interfaces. Before self-healing heat treatment, as shown in Fig. 8a, a few microcracks existed in the SAZ–YSZ interface. After self-healing heat treatment, the interface of the SAZ and YSZ coatings was well-bonded

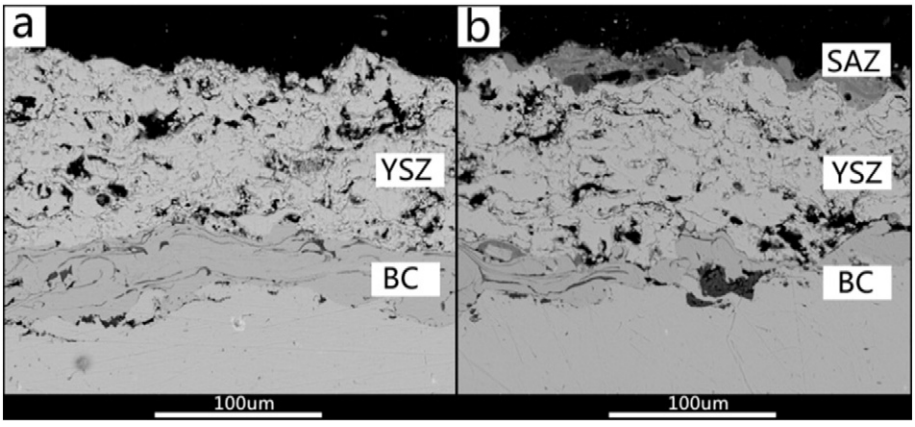

Fig. 4. SEM images for cross-section morphologies of (a) an as-sprayed YSZ-TBC sample and (b) an as-sprayed SAZ-TBC sample.

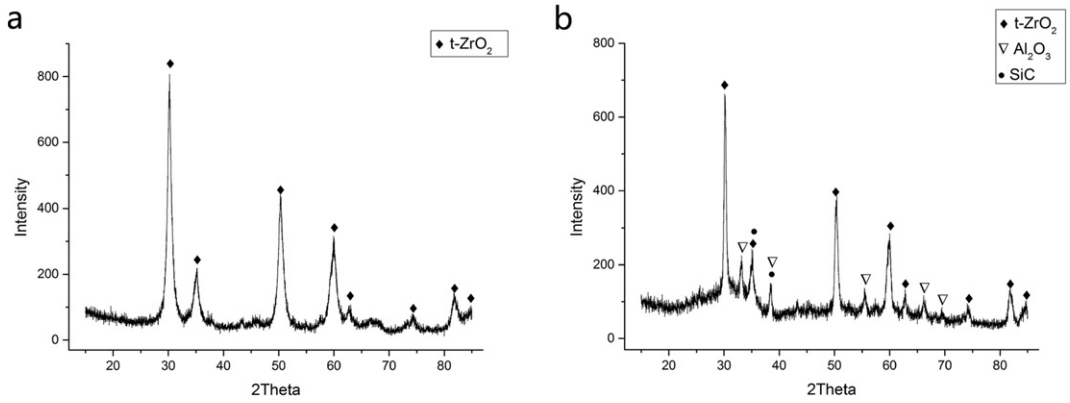

Fig. 5. XRD patterns of the as-sprayed YSZ coating and SAZ coating.

(Fig. 8b), showing no clear evidence of cracks or potential crack nucleation.

Electrochemical test results (Fig. 10) further confirmed the filling and sealing effect in SAZ coatings after heat treatment. The filling and sealing effects of SAZ coatings were the result of an implicit relationship between corrosion current densities and porosity, where the samples with lower porosity showed lower corrosion current densities in the electrochemical test results. According to a study we conducted previously [9], the electrolytes in pores and cracks worked as a circuit in the coatings, promoting increased corrosion current densities in the electrochemical test results. Therefore, when pores and cracks in composite coatings were filled and sealed, the corresponding corrosion current densities decreased. The electrochemical test polarization curves and corrosion current densities are depicted in Fig. 10. The corrosion current densities for SAZ TBC samples decreased by 70.68% after self-healing heat treatment, providing solid evidence of filling and sealing effect.

4.2. Oxidation resistance and function of SAZ constituents

The self-diffusion of oxygen in Al_2O_3 has been of scientific and technological interest for some time [45]. The oxygen diffusion coefficient in Al_2O_3 is approximately ~10^{-27} m^2/s at 1127 °C, suggesting that Al_2O_3 is a very good oxidation-resistance material [15,45–48]. Al_2O_3 can reduce the oxidation rate of metallic coatings [13], but the thermal expansion mismatch between the coating and underlying YSZ layers makes the coating spall easily under temperature fluctuations.

YSZ has a larger thermal expansion coefficient than most of other oxides, so YSZ in self-healing coatings narrows the thermal expansion coefficient mismatch between self-healing layers and YSZ layers. However, according to Fox [47], YSZ is a good conductor of oxygen ions at high temperatures [13]. The diffusion coefficient of oxygen ions in YSZ is approximately ~10^{-10} m^2/s at 1127 °C [47,49–51].

Fast-path diffusion of oxygen occurs when there are defects in coatings [52], and oxygen diffusion coefficient can be regarded as infinite

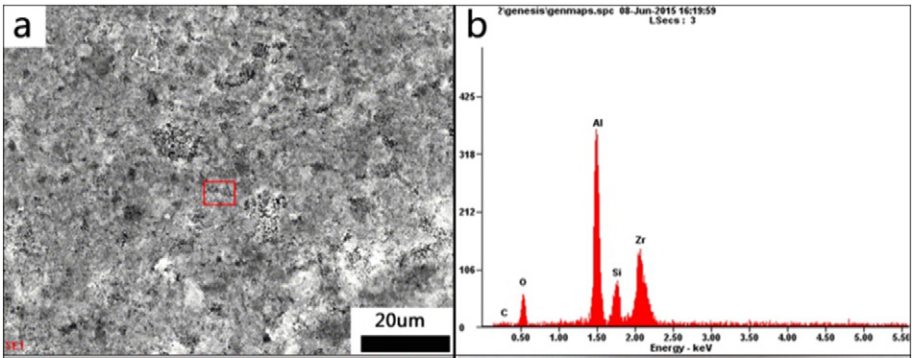

c ement	Wt%	At%
CK	05.57	15.34
OK	15.42	31.86
AlK	22.06	27.02
SiK	06.34	07.46
ZrK	50.61	18.34
Matrix	Correction	ZAF

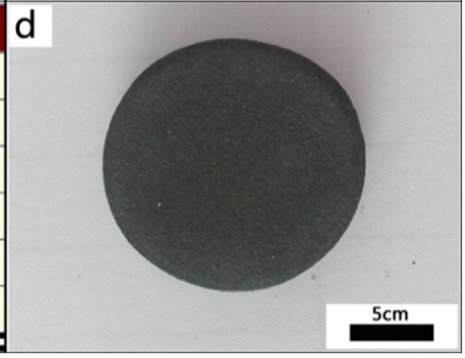

Fig. 6. (a) Top-view SEM image of an as-sprayed SAZ-TBC sample, (b) EDS map for box area in (a), (c) the elements percentage for the SAZ coating and (d) the top-view recorded by camera for an as-sprayed SAZ-TBC sample.

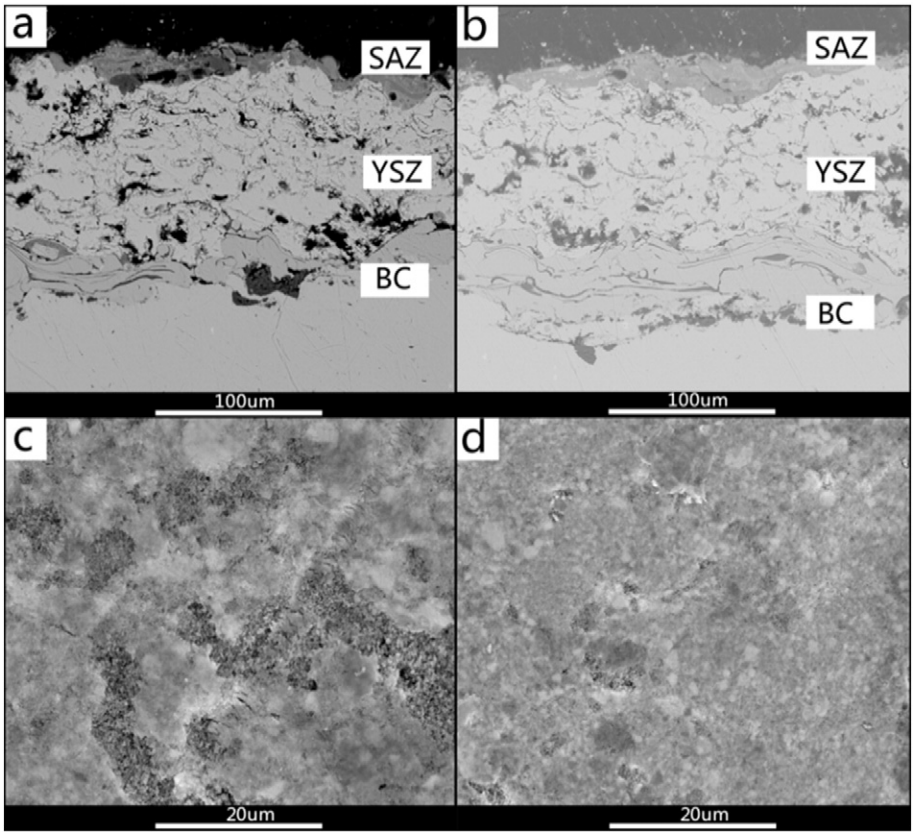

Fig. 7. SEM images for cross-section morphologies and top surface morphologies of SAZ-TBC samples (a), (c) before and (b), (d) after self-healing heat treatment.

when oxygen diffuses in air. For this reason, cracks and pores decrease the oxidation resistance of coatings. To this effect, the filling and sealing process caused by the oxidation of self-healing agent improves the oxidation resistance of coatings. SiO_2 is currently quite commonly used as an oxidation barrier coating [53–55], and the diffusion coefficient of interstitial O_2 is approximately ~10^{-13} m^2/s [56] at 1127 °C, so SiO_2 likely can fulfill healing functions and improve coating oxidation resistance even though its oxygen diffusion coefficient is much higher than that of Al_2O_3.

4.3. Oxide growth in coatings at high temperatures

Oxidation test mass gain records revealed the growth rate of the oxide in tested samples. As shown in Fig. 11, after 20 cycles of high-temperature oxidation, the average mass gain of the samples with BC was only 5.90 mg/cm^2 while the average mass gain of the conventional TBC samples was 5.53 mg/cm^2. The YSZ coatings, which were fabricated by APS, only slightly improved the oxidation resistance of the TBC samples (Section 4.2). The average mass gain of the samples with SAZ coatings was 3.75 mg/cm^2, 67.81% of the average mass gain for conventional TBC samples. According to the results discussed in Section 4.1, the mass gain caused by oxidation of self-healing agent was about 0.25 mg/cm^2, therefore the real mass gain caused by TGO growth was 3.50 mg/cm^2 (63.29% of the average mass gain for conventional TBC samples.) These results imply that SAZ layers enhanced the oxidation resistance of the TBC system, while YSZ layers contribute less to oxidation resistance.

Cross-sectional SEM images of both SAZ TBC and YSZ TBC samples after every 5 h of high-temperature oxidation are shown in Fig. 10, and the results of IPP analysis of TGO percentages in BC are listed in

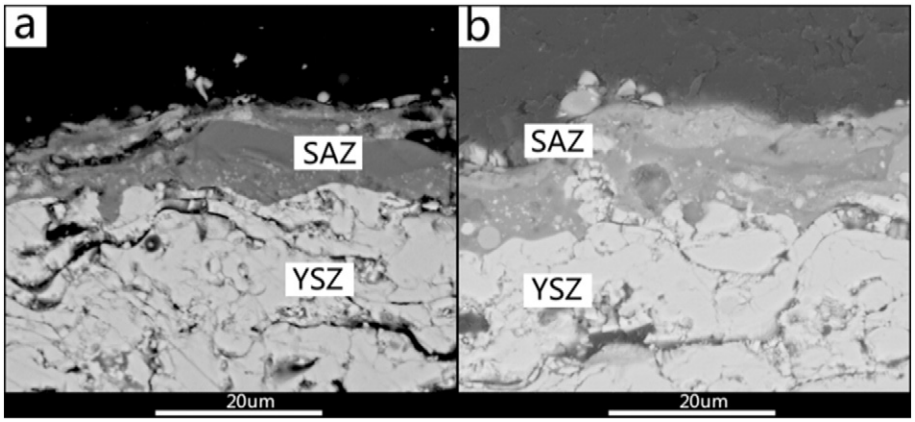

Fig. 8. Magnified SEM images for cross-section morphologies of SAZ–YSZ interface (a) before and (b) after self-healing heat treatment.

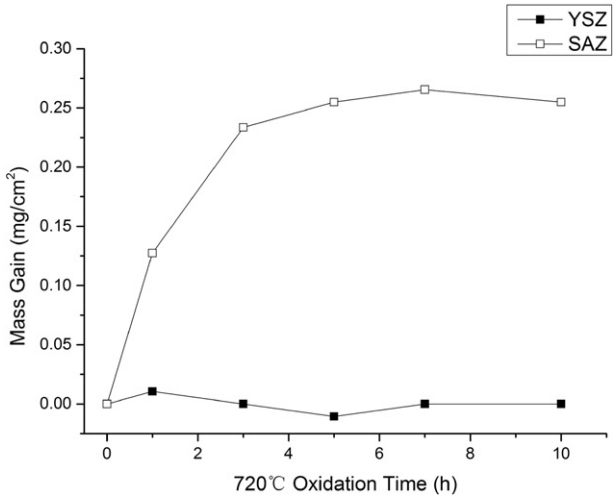

Fig. 9. Oxidation kinetic curve for SAZ-TBC and YSZ-TBC samples for 10 h at 720 °C.

Table 4. Results showed that the TGO percentage in SAZ TBC samples was lower than that of YSZ TBC samples at every stage, in accordance with the mass gain results. Both the mass gain test and TGO analysis provided the same conclusion: that SAZ coatings enhanced the high-temperature oxidation resistance of the TBC system.

To better understand TGO growth, we analyzed the following four stages of the high-temperature cyclic oxidation process.

1) After first five oxidation cycles, TGO layers were present in both types of TBC samples. The EDS results of TGO grown in YSZBC interfaces (area "d" in Fig. 11a and d) showed that the Al element had the most intensive peak, though there also were peaks for Ni, Cr, and O [3,57]. The Pt element present in the EDS results was the result of Pt spraying before tests, so it was negligible. These results agree with those reached by previous studies [3,57–59]. The initial TGO in the ceramic–metal interface was mainly Al_2O_3 [60–62].
2) After 10 oxidation cycles, the other type of TGO was found in conventional and SAZ TBC samples (Fig. 12). The EDS map (Fig. 11c) for zone "c" in Fig. 11a showed intensive peaks for Cr and O elements, confirming that the external oxide was mainly Cr_2O_3. According to the magnified SEM images of Cr_2O_3 TGO (Fig. 15), the material had porous structure and was susceptible to crack nucleation and propagation [2]. Cracks created more paths for inward diffusion of oxygen, which promoted the growth of Cr_2O_3 TGO. In turn, the growth of Cr_2O_3 TGO induced more cracks. Because Cr came from the BC and the substrate, Cr_2O_3 TGO seemed grow inward to the substrate. As shown in zone "C" in Fig. 12b, a portion of the Cr_2O_3 TGO penetrated the BC. The first spallation was found in the surfaces of the YSZ TBC samples after 10 oxidation cycles according to our records.
3) After 15 oxidation cycles, the TGO percentage reached up to 84.42%, and severe cracks were found in the YSZ TBC cross-section SEM images (Fig. 12c). The TGO percentage of SAZ TBC samples (Fig. 13c) was 52.22%, similarly to YSZ TBC samples after 10 oxidation cycles (where TGO percentage was 58.17%).The severe cracks very likely were a result of connections between oxide-induced cracks and pre-existing discontinuities in the YSZ layers, as shown in Fig. 15.
4) YSZ TBC samples had completely peeled off after 20 oxidation cycles, leaving only the TGO layer on the substrates. These substrates may have reacted with oxygen, causing the TGO to continue to thicken and form clear corrosion boundaries. Cr_2O_3 TGO and oxide-induced cracks were both found in SAZ TBC samples, and spallation first occurred on the surfaces of SAZ TBC samples after 18 oxidation cycles.

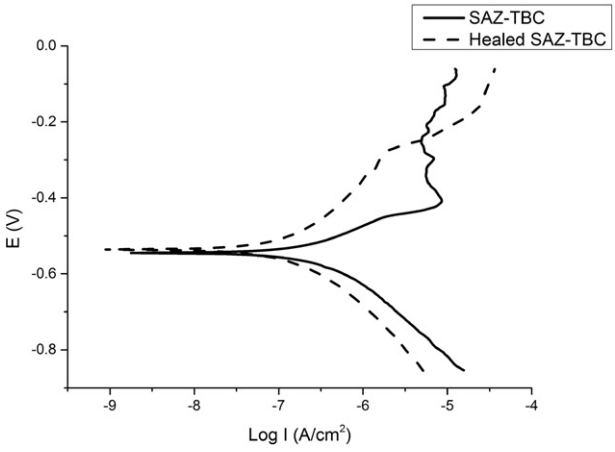

Fig. 10. Polarization curves and corrosion current for samples with as-sprayed SAZ-TBC coatings and healed SAZ-TBC coatings.

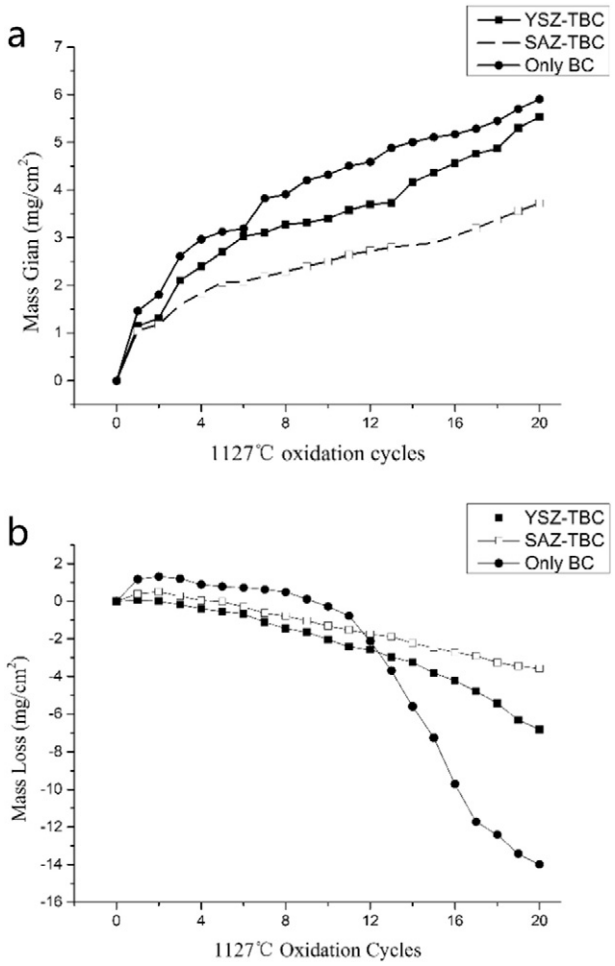

Fig. 11. Oxidation kinetic curves of the samples at 1127 °C in air for 20 h: (a)mass gain vs. time; (b) mass loss vs. time.

We observed two main types of TGO:Al_2O_3 TGO, which was initially found in TBC samples, and Cr_2O_3 TGO. According to Busso [57–59], the first type of TGO is internally grown. The growth rate of the internal oxide layer is likely controlled by the inward diffusion of oxygen, mostly toward the TGO-metal interface along grain boundaries [63]. Externally grown oxide, Cr_2O_3 TGO, causes external oxidation controlled by the outward diffusion of Cr cations along the boundaries of the alumina that comprised the existing TGO by reacting with oxygen anions at the interface between the TGO layer and the ceramic layer [57]. The EDS

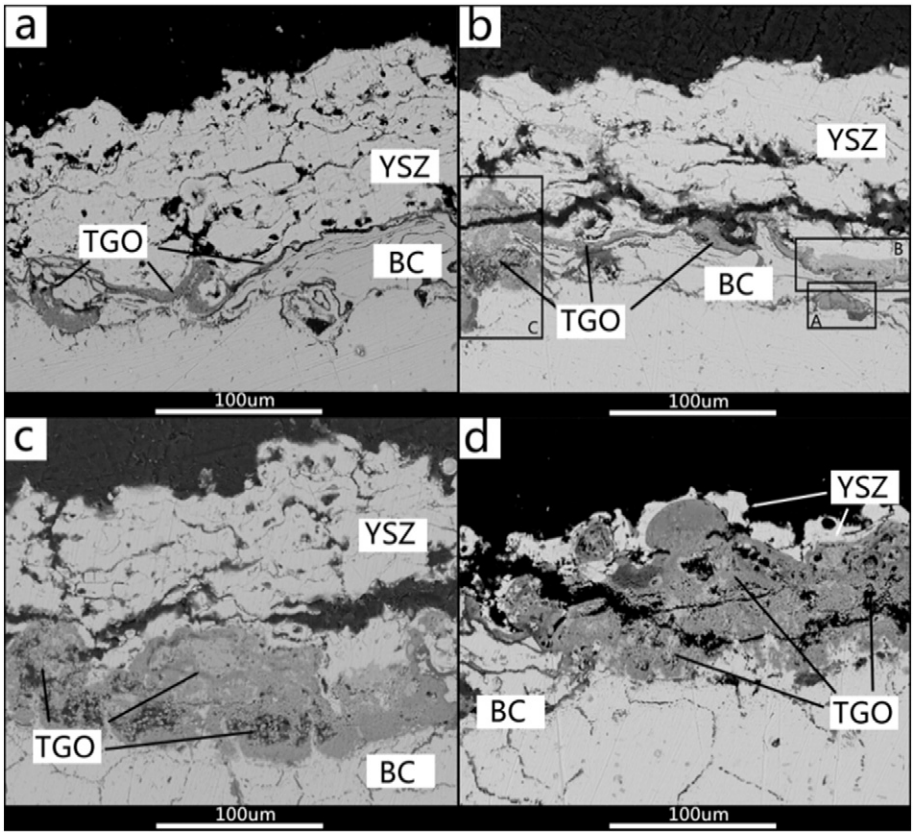

Fig. 12. Cross-section SEM images of YSZ TBC samples after high temperature oxidation for (a) 5 h, (b) 10 h, (c) 15 h and (d) 20 h.

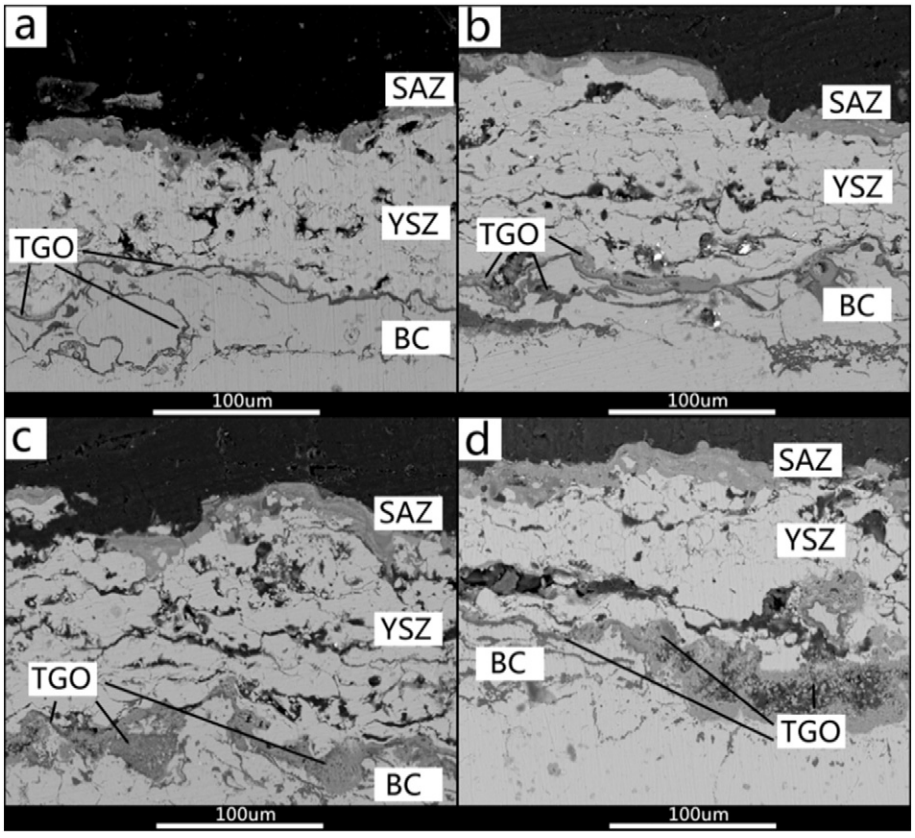

Fig. 13. Cross-section SEM images of SAZ TBC samples after high temperature oxidation for (e) 5 h, (f) 10 h, (g) 15 h and (h) 20 h.

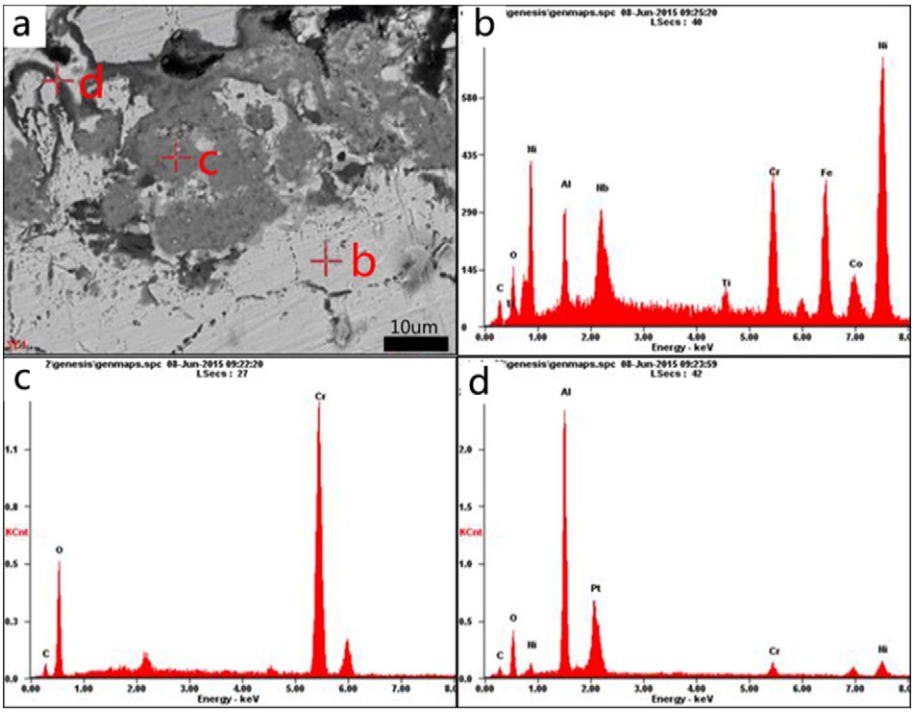

Fig. 14. (a) SEM image for a cross-section morphology of TGO in BC and (b–d) EDS maps for different areas in (a).

results shown in Fig. 14b show where the material zone "b" in Fig. 14a belongs to the substrates. Basically, Cr cations not only came from the BC, but also from the substrates. If Cr cations only came from BC, as suggested by Chen [2], the Cr_2O_3 TGO would only exist as external TGO in the ceramic–TGO interface instead of almost replacing the BC alloy after 20 h of high-temperature oxidation. TGO-induced cracks grew and then promoted further growth of TGO. Crack nucleation and propagation in these two TBCs were related to the growth and coalescence of oxide-induced cracks, connecting with pre-existing discontinuities in the YSZ layers.

4.4. Spallation resistance during oxidation

The mass loss records reflect the mass change of samples without crucibles after isothermal oxidation, and reveal the spalling degree of the samples. As shown in Fig. 11(b), SAZ TBC samples lost less mass in same period than other samples. After 20 oxidation cycles, the average mass loss of SAZ TBC samples was 3.58 mg/cm^2, but reached 6.83 mg/cm^2 for conventional YSZ-TBC samples. The mass gain caused by self-healing agent oxidation is about 0.25 mg/cm^2, so the true value of average mass loss for SAZ TBC samples was 3.83 mg/cm^2–56.08% of the conventional TBC samples.

Three types of cracks nucleated and propagated in the samples: those in the SAZ coatings, YSZ layers, and TGO.

1) In the cross-section morphologies of SAZ coatings after 20 oxidation cycles, a portion of the self-healing layers escaped the TBCs, leaving vertical cracks under the spallation position. This phenomenon was one of the reasons for vertical cracks.
2) The porosity of as-sprayed YSZ coatings (Fig. 4) fabricated by APS was about 10%–20% [64–66]. These defects in as-sprayed coatings tended to evolve into cracks during high-temperature oxidation. The driving force of crack propagation was two kinds of stress: thermal stress in YSZ layers due to thermal cycles [62], and heavy stress due to TGO growth [67]. Bulk spallation in YSZ layers occurred when horizontal cracks connected to vertical cracks.
3) As shown in Fig. 15, the porous structure of Cr_2O_3 TGO was also likely to induce cracks. These cracks occurred due to large compress stress inside the TGO [68], which was also influenced by the undulation amplitude and thickness of TGO layers [69].

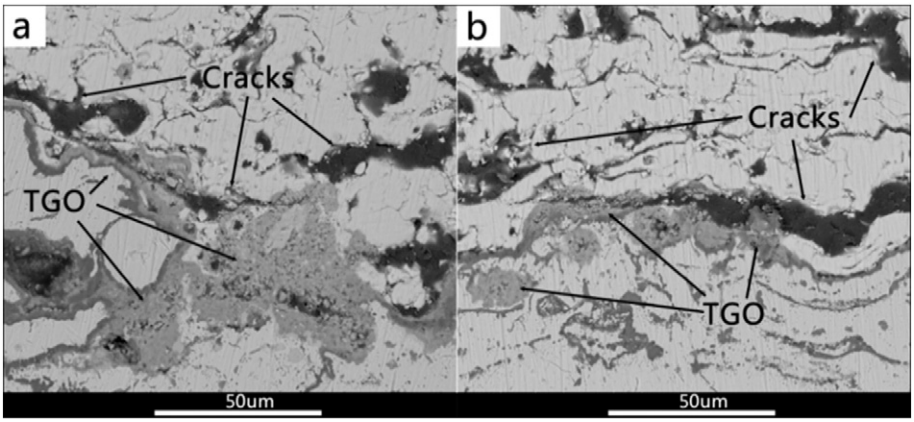

Fig. 15. Cracks nucleation and propagation in (a) a YSZ-TBC sample and (b) a SAZ-TBC sample after oxidation for 15 h at 1127 °C.

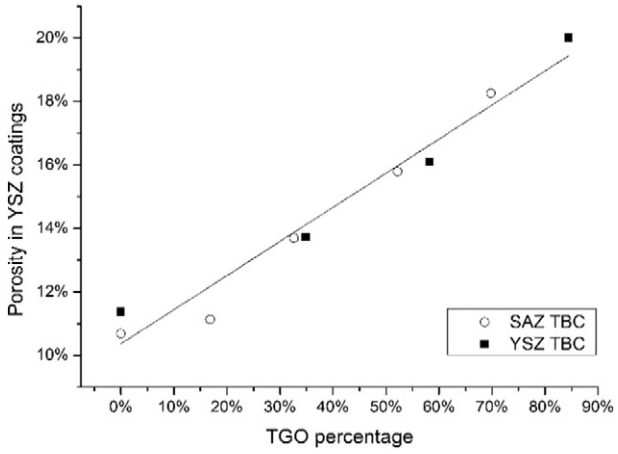

Fig. 16. Correlation between TGO percentage in BCs and porosity in YSZ coatings of YSZ TBC samples and SAZ TBC samples.

Initial spallation consistently occurred in all YSZ layers, so, in theory, connections between YSZ layer cracks may have led to TBC failure. A linear relationship between TGO percentage TBC sample porosity was found, as shown in Fig. 16. The porosity of YSZ coatings increased the crack nucleation and propagation, and the linear relationship between the two showed where TGO reduced the lifetime of TBC. TGO was less involved in the SAZ TBC samples, so SAZ prolonged the lifetime of the TBC system.

A similar conclusion can be drawn based on the stress intensity we observed during the experiment. Evans et al. [70] posed the following method of calculating stress intensity factor K at the crack tip in the TBC, where cracks occur near the TGO:

$$K = \frac{3}{2(1+\nu)\sqrt{\pi}}\left(\frac{R}{a}\right)^{c}\frac{E(m-1)}{3(1-\nu)m}\left(\frac{h}{R}\right)\sqrt{R} \quad (2)$$

K stress intensity factor
h TGO thickness
a crack length
R radius of an individual splat of grain at the interface
m ratio of volume change
E Young's modulus of the TBC
ν Poisson's ratio
c constant.

The equivalent TGO thickness is defined as follows [71]:

$$h = \frac{\sum A_{TGO}}{\sum L_{TGO\text{-}BC}} = \frac{P_{TGO}A_{BC}}{\sum L_{TGO\text{-}BC}} \quad (3)$$

Table 5
Normalized stress intensity factor evaluation base on ideal mode.

	Normalized Stress intensity factor in 1127 °C oxidation test			
	5 h	10 h	15 h	20 h
SAZ TBC	0.29	0.56	0.52	Spallation
YSZ TBC	0.60	1.00	Spallation	Spallation

where the A_{TGO}, $L_{TGO\text{-}BC}$, $P_{TGO,}$ and A_{BC} are the cross-sectional TGO area, the cross-sectional length of the TGO-BC interface, TGO percentage, and BC area, respectively.

Assume a SAZ TBC sample and a YSZ TBC sample prepared under completely identical conditions with identical properties. A crack in each sample, in the same shape and same position, can be used to evaluate stress intensity in the samples. After a certain amount of high-temperature oxidation, the only difference between the two samples is the TGO percentage, which was decided by the oxidation resistance of each sample. Eqs. (2) and (3), as such, yield the following:

$$\frac{K_{SAZ}}{K_{YSZ}} = \frac{P_{TGOSAZ}}{P_{TGOYSZ}} \quad (4)$$

where K_{SAZ} and K_{YSZ} are stress intensity factors of SAZ TBC and YSZ TBC, and P_{TOGSAZ} and P_{TGOYSZ} are TGO percentages of SAZ TBC and YSZ TBC, respectively. The normalized results of stress intensity factor of TBC samples calculated in this manner at different stages of high-temperature oxidation are listed in Table 5. Though this is a very ideal mode for evaluating K, the results still also be used to elucidate the relationship between TGO and stress intensity in the TBC, and can further be used to explain the reason that initial spallation occurred much earlier in YSZ TBC samples in our experiment.

5. Conclusion

In this paper, a comparative study of the high temperature cyclic oxidation behavior of the SAZ TBC and the YSZ TBC has been carried out, using mass gain and mass loss to quantitatively assess the oxidation resistance and spallation resistance of two kinds of TBCs. The following important conclusions can be made.

1) Both SEM images and corrosion current densities of the SAZ TBC showed that SiC can fill and seal pores and cracks in SAZ coatings heated at 720 °C for 10 h. Self-healing effect caused the porosity of SAZ coatings to drop 76.71%.
2) The mass gain results reveal that the oxidation resistance of SAZ TBC is better than that of YSZ TBC, because the mass gain of SAZ TBC samples decreased 36.71% on average after 20 oxidation cycles at 1127 °C compared to YSZ TBC.
3) Mass loss results revealed that the spallation resistance of the SAZ TBC was better than that of YSZ TBC; the mass loss of SAZ TBC

Table 4
Porosity and TGO area percentage for YSZ-TBC and SAZ-TBC samples.

		Porosity in SAZ layer	Porosity in YSZ layer	TGO area percentage in BC
YSZ-TBC	As-sprayed	–	11.37%	–
	720 °C for 10 h	–	11.01%	–
	1127 °C for 5 h	–	13.73%	34.88%
	1127 °C for 10 h	–	16.10%	58.17%
	1127 °C for 15 h	–	20.01%	84.42%
	1127 °C for 20 h	–	Spallation	88.05%
SAZ-TBC	As-sprayed	9.19%	10.68%	–
	720 °C for 10 h	2.14%	10.62%	–
	1127 °C for 5 h	4.17%	11.13%	16.84%
	1127 °C for 10 h	1.96%	13.69%	32.65%
	1127 °C for 15 h	1.90%	15.79%	52.22%
	1127 °C for 20 h	2.52%	18.26%	69.80%

samples decreased 43.78% on average after 20 oxidation cycles at 1127 °C compared to YSZ TBC.

4) An ideal model was been established in this study for evaluating the stress intensity of TBC samples. The results indicate that enhanced oxidation resistance enhances the lifetime of the TBC system.

To sum up, SAZ coatings could enhance oxidation resistance and spallation resistance of the TBC system greatly during high temperature oxidation.

References

[1] M.G. Nitin, P. Padture, E.H. Jordan, Science 296 (2002) 280–284.
[2] W.R. Chen, X. Wu, B.R. Marple, D.R. Nagy, P.C. Patnaik, Surf. Coat. Technol. 202 (2008) 2677–2683.
[3] P. Poza, J. Gómez-García, C.J. Múnez, Acta Mater. 60 (2012) 7197–7206.
[4] N. Narimani, M. Saremi, Ceram. Int. 41 (2015) 13810–13816.
[5] L.I.N. Zhu, N. Zhang, R. Bolot, H. Liao, C. Coddet, Surf. Rev. Lett. 22 (2015) 1550061.
[6] Z. Fan, K. Wang, X. Dong, W. Duan, X. Mei, W. Wang, J. Cui, J. Lv, Surf. Coat. Technol. 277 (2015) 188–196.
[7] L. Wei, H. Peng, F. Jia, L. Zheng, S. Gong, H. Guo, Surf. Coat. Technol. 276 (2015) 721–725.
[8] H.M. Tawancy, A.I. Mohammed, L.M. Al-Hadhrami, H. Dafalla, F.K. Alyousef, Oxid. Met. 84 (2015) 527–539.
[9] H. Guo, Y. Cui, H. Peng, S. Gong, Corros. Sci. 52 (2010) 1440–1446.
[10] T. Akatsu, T. Kato, Y. Shinoda, F. Wakai, Surf. Coat. Technol. 223 (2013) 47–51.
[11] Y. Li, Y. Xie, L. Huang, X. Liu, X. Zheng, Ceram. Int. 38 (2012) 5113–5121.
[12] A. Keyvani, M. Saremi, M.H. Sohi, J. Alloys Compd. 509 (2011) 8370–8377.
[13] K. Zhang, S. Ning, C. Ren, X. Luo, L. Dong, H. Chen, Y. He, Surf. Coat. Technol. (2015).
[14] W.R. Chen, X. Wu, B.R. Marple, R.S. Lima, P.C. Patnaik, Surf. Coat. Technol. 202 (2008) 3787–3796.
[15] J. Yao, Y. He, D. Wang, H. Peng, H. Guo, S. Gong, Corros. Sci. 80 (2014) 37–45.
[16] M. Saremi, Z. Valefi, Ceram. Int. 40 (2014) 13453–13459.
[17] P. Cordier, F. Tournilhac, C. Soulie-Ziakovic, L. Leibler, Nature 451 (2008) 977–980.
[18] D.Y. Wu, S. Meure, D. Solomon, Prog. Polym. Sci. 33 (2008) 479–522.
[19] S.R.W.E.N. Brown, N.R. Sottos, J. Mater. Sci. 39 (2004) 1703–1710.
[20] D.D. Vincenzo Amendola, S. Polizzi, J. Shen, K.M. Kadish, M.J.F. Calvete, M. Hanack, M. Meneghetti, J. Phys. Chem. C 113 (2009) 8688–8695.
[21] M. Nosonovsky, R. Amano, J.M. Lucci, P.K. Rohatgi, Phys. Chem. Chem. Phys. 11 (2009) 9530–9536.
[22] D.G. Shchukin, M. Zheludkevich, K. Yasakau, S. Lamaka, M.G.S. Ferreira, H. Möhwald, Adv. Mater. 18 (2006) 1672–1678.
[23] W. Ni, Y.-T. Cheng, D.S. Grummon, Appl. Phys. Lett. 80 (2002) 3310.
[24] H. Mihashi, T. Nishiwaki, J. Adv. Concr. Technol. 10 (2012) 170–184.
[25] V. Wiktor, H.M. Jonkers, Cem. Concr. Compos. 33 (2011) 763–770.
[26] H.M. Jonkers, A. Thijssen, G. Muyzer, O. Copuroglu, E. Schlangen, Ecol. Eng. 36 (2010) 230–235.
[27] W. Zhong, W. Yao, Constr. Build. Mater. 22 (2008) 1137–1142.
[28] H.-W. Reinhardt, M. Jooss, Cem. Concr. Res. 33 (2003) 981–985.
[29] M.R. Hansen, M. Krogsgaard, H. Birkedal, J. Mater. Chem. B 2 (2014) 8292–8297.
[30] J.B. Ferguson, B.F. Schultz, P.K. Rohatgi, JOM 66 (2014) 866–871.
[31] Z.Z. Guo Liang Li, H.M. Hwald, D.G. Shchukin, ACS Nano 7 (2013) 2470–2478.
[32] S. Bode, et al., Polym. Chem. 4 (2013) 4966.
[33] R.P. Wool, Soft Matter 4 (2008) 400.
[34] A. Kumar, L.D. Stephenson, J.N. Murray, Prog. Org. Coat. 55 (2006) 244–253.
[35] S.V. Lamaka, M.L. Zheludkevich, K.A. Yasakau, R. Serra, S.K. Poznyak, M.G.S. Ferreira, Prog. Org. Coat. 58 (2007) 127–135.
[36] M.L. Zheludkevich, K.A. Yasakau, A.C. Bastos, O.V. Karavai, M.G.S. Ferreira, Electrochem. Commun. 9 (2007) 2622–2628.
[37] D.V. Andreeva, D. Fix, H. Mohwald, D.G. Shchukin, Adv. Mater. 20 (2008) 2789–2794.
[38] V. Sauvant-Moynot, S. Gonzalez, J. Kittel, Prog. Org. Coat. 63 (2008) 307–315.
[39] J.H. Park, P.V. Braun, Adv. Mater. 22 (2010) 496–499.
[40] M. Samadzadeh, S.H. Boura, M. Peikari, S.M. Kasiriha, A. Ashrafi, Prog. Org. Coat. 68 (2010) 159–164.
[41] M. Samadzadeh, S.H. Boura, M. Peikari, A. Ashrafi, M. Kasiriha, Prog. Org. Coat. 70 (2011) 383–387.
[42] S.V. Raj, M. Singh, R.T. Bhatt, High Temperature Lightweight Self-healing Ceramic Composites for Aircraft Engine Applications, 2014.
[43] C. Kaplin, M. Brochu, Appl. Surf. Sci. 301 (2014) 258–263.
[44] J. Li, L. Ecco, M. Fedel, V. Ermini, G. Delmas, J. Pan, Prog. Org. Coat. 87 (2015) 179–188.
[45] A.H. Heuer, J. Eur. Ceram. Soc. 28 (2008) 1495–1507.
[46] T. Nakagawa, I. Sakaguchi, N. Shibata, K. Matsunaga, T. Mizoguchi, T. Yamamoto, H. Haneda, Y. Ikuhara, Acta Mater. 55 (2007) 6627–6633.
[47] A.C. Fox, T.W. Clyne, Surf. Coat. Technol. 184 (2004) 311–321.
[48] J. Yao, Y. He, D. Wang, H. Peng, H. Guo, S. Gong, Appl. Surf. Sci. 286 (2013) 298–305.
[49] A.E. Ken Suzuki, R. Miura, Y. Oumi, H. Takaba, M. Kubo, A. Chatterjee, A. Fahmi, A. Miyamoto, Appl. Surf. Sci. 130–132 (1998) 545–548.
[50] R.L. González-Romero, J.J. Meléndez, J. Alloys Compd. 622 (2015) 708–713.
[51] R.L. González-Romero, J.J. Meléndez, D. Gómez-García, F.L. Cumbrera, A. Domínguez-Rodríguez, Solid State Ionics 219 (2012) 1–10.
[52] X.Y. Zhang, D.J. Cherniak, E.B. Watson, Chem. Geol. 235 (2006) 105–123.
[53] Z.-Q. Fu, C.-B. Wang, C.-H. Tang, H.-S. Zhao, J.-C. Robin, Nucl. Eng. Des. 265 (2013) 867–871.
[54] W.E.L.S. Zhang, J. Eur. Ceram. Soc. 23 (2003) 1215–1221.
[55] O.-S.K. Young-Hag Koh, S.-H. Hong, H.-E. Kim, S.-K. Lee, J. Eur. Ceram. Soc. 21 (2001) 2407–2412.
[56] K. Kajihara, T. Miura, H. Kamioka, M. Hirano, L. Skuja, H. Hosono, Mater. Sci. Eng. B 173 (2010) 158–161.
[57] J.L.E.P. Busso, S. Sakurai, M. Nakayama, Acta Mater. 49 (2001) 1515–1528.
[58] E.P. Busso, Z.Q. Qian, M.P. Taylor, H.E. Evans, Acta Mater. 57 (2009) 2349–2361.
[59] E.P. Busso, H.E. Evans, Z.Q. Qian, M.P. Taylor, Acta Mater. 58 (2010) 1242–1251.
[60] J. Schwarzer, D. Löhe, O. Vöhringer, Mater. Sci. Eng. A 387-389 (2004) 692–695.
[61] D.S. Balint, S.S. Kim, Y.-F. Liu, R. Kitazawa, Y. Kagawa, A.G. Evans, Acta Mater. 59 (2011) 2544–2555.
[62] S. Kyaw, A. Jones, T. Hyde, Eng. Fail. Anal. 27 (2013) 150–164.
[63] M.K.L.J. Balmain, A.M. Huntz, Mater. Sci. Eng. A 224 (1997) 87–100.
[64] C.F.B. Siebert, R. Vaben, D. Sto Èver, J. Mater. Process. Technol. 92-93 (1999) 217–223.
[65] A. Portinha, V. Teixeira, J. Carneiro, M.G. Beghi, C.E. Bottani, N. Franco, R. Vassen, D. Stoever, A.D. Sequeira, Surf. Coat. Technol. 188-189 (2004) 120–128.
[66] A. Scrivani, G. Rizzi, C.C. Berndt, Mater. Sci. Eng. A 476 (2008) 1–7.
[67] H.-Y. Qi, X.-G. Yang, Comput. Mater. Sci. 57 (2012) 38–42.
[68] R. Kitazawa, H. Kakisawa, Y. Kagawa, Surf. Coat. Technol. 238 (2014) 68–74.
[69] M. Martena, D. Botto, P. Fino, S. Sabbadini, M.M. Gola, C. Badini, Eng. Fail. Anal. 13 (2006) 409–426.
[70] M.Y.H.A.G. Evans, J.W. Hutchinson, Prog. Mater. Sci. 46 (2001) 249–271.
[71] W.R. Chen, X. Wu, B.R. Marple, P.C. Patnaik, Surf. Coat. Technol. 201 (2006) 1074–1079.